encit 2020

ABCM Associação Brasileira de Engenharia e Ciências Mecânicas

18th Brazilian Congress of Thermal Sciences and Engineering
November 16-20, 2020 (Online)

ENC-2020-0479
POTENTIAL ENERGY OF ABANDONED OIL WELLS FOR DEPLOYMENT OF NEW GEOTHERMAL POWER PLANTS

Thiago Croisfelt Batista
Júlio César Passos
Edson Bazzo
Federal University of Santa Catarina, Department of Mechanical Engineering, 88040-900 - Florianópolis – SC
t.croisfelt.batista@gmail.com, julio.passos@ufsc.br, e.bazzo@ufsc.br

Abstract. *The present paper aimed to estimate the geothermal potential of the extended lifecycle of four non productive onshore oil wells in the Brazilian states of Mato Grosso, Paraná, Rio Grande do Norte and Santa Catarina. A transient numerical model was designed, deploying a finite volume method, coupling the lithosphere thermal behavior to the recirculating water stream inside each studied wellbore. Heat power potentials between 287.4 and 411.0 kW were estimated for one month of elapsed operating time, decreasing to the range between 157.0 and 235.4 kW at the last simulated year. The heated water achieved temperatures between 89 and 105 ºC. Process losses were also analyzed, indicating heat escape to the upper layers of the soil, whose rates were up to 80 kW. Also, assumptions were discussed, leading to the finding of simplifications that may result in distorted results for this kind of study.*

Keywords: *Brazilian oilfield, Geothermal energy, Abandoned oil well, Potential heat power.*

1. INTRODUCTION

Geothermal wells have very similar structure of oil wellbores, both deploy same drilling technologies and use to be built by the same companies worldwide (REN21, 2017). This fact may highlight the opportunity of reusing depleted structures from an industrial cycle into another sector, for example, deploying new geothermal power plants on abandoned oil wells. Many studies have been reported in this context, evaluating concepts and implications of this type of recycling, such as the works of Davis and Michaelides (2009), Bu *et al.* (2012), Cheng *et al.* (2013), Wight and Bennet (2015) and Noorollahi *et al.* (2015). Recently, *Yang et al.* (2017) reported the construction of real power plant reusing a pair of abandoned wells in the Chinese oilfield.

However, there is no geothermal power plant in Brazil, even with a developed oil and gas industry and up to 22,756 registered onshore well drillings in the Brazilian oilfield, 9,514 of them with a non productive or abandoned status (SDT-ANP, 2017). Indeed only few studies were found covering this type of new developments (Batista, 2019).

In this context, the present work aimed evaluate the transient behavior of four simulated onshore oil wells, these, in their extended lifecycle, hypothetically recovering geothermal heat to new power plants.

2. METHODOLOGY

2.1 Nature of the case studies

Four abandoned oil wells were selected to be studied, here referred by the abbreviation of the corresponding Brazilian state, where they are placed, as shown in Tab. 1. All selected wells were vertically drilled and had in 2017 a non productive status (SDT-ANP, 2017).

Table 1. General characteristics of the four selected cases study.

Reference	ANP Code[(1)]	State[(1)]	Depth (m) [(1)]	$\lvert\nabla T_{geo}\rvert$ (ºC/km) [(1)]	BHT^0 (ºC) [(1)]	T_{amb} (ºC) [(2)]
MT	1-BRSA-1204-MT	Mato Grosso	6,053.5	18.08	146.62	23.9
PR	1API 0001 PR	Paraná	5,902.0	20.57	144.44	20.8
RN	6-BRSA-588-RN	Rio Grande do Norte	4,729.2	38.87	161.42	28.0
SC	1GO 0001 SC	Santa Catarina	4,102.8	33.86	155.82	16.9

[(1)]Source: SDT-ANP (2017), [(2)]Source: Merkel (2017).

In this study, once geothermal power plants have unstoppable heat supply (Dipippo, 2012), the power oscillations were neglected and atmospheric temperature (T_{amb}) were considered to be constant and equal to the annual average temperature of the well locations.

The drilling and casing dimensions, in addition to the geological formation data, were recovered from the borehole logging report (SDT-ANP, 2017). The lithology log, specifically, were filtered and simplified (Barcelos, 2017, and Noorollahi *et al.*, 2015) to contain up to 20 groups of rocks along the entire depth of the well numeric model. This enabled data to be inputted into the coded algorithms (Batista, 2019). Moreover, the properties of rocks depend on factors such as porosity, pore content, age of formation, lithospheric pressure and temperature. Thus, the same mineral can have different properties if it is extracted from different regions of the planet (DiPippo, 2012, and Schön, 2015). Given the difficulty of mapping such aspects, the rocks were taken as homogeneous and isotropic (DiPippo, 2012, and Hamza *et al.*, 2005) and their properties (Tab. 2) were defined by the center values found in the literature.

Table 2. Thermodynamic properties considered for rocks in the studied wells.

Rock layer	ρ (kg/m^3)	k (W/m.K)	c_p (J/kg.K)
Basalt	2,800	1.95	880
Conglomerate	2,475	3.36	1,575
Diabase	2,950	2.64	910
Dolomite	2,625	3.62	1,000
Limestone	2,710	2.29	930
Metamorphic	2,950	3.50	945
Sandstone	2,150	2.90	745
Shale	2,275	2.30	1,180

Source: Compiled from Bergman *et al.* (2011) and Schön (2015).

2.2 Numerical model

In order to recover geothermal heat from the ground rocks, a double-pipe concept (as exemplified by previous works, such as by Cheng *et al.* in 2013) was modeled, so it would be possible to have only a single well for both injection and extraction of thermal fluid from the Earth's crust. Then the fully implicit Finite Volume Method was used to solve the hydrodynamic problem in the inner upstream and annular downstream flows (using the upwind scheme, Maliska, 2004), as well as to solve the thermal problem in the entire domain, including the lithosphere portion (see Fig. 1).

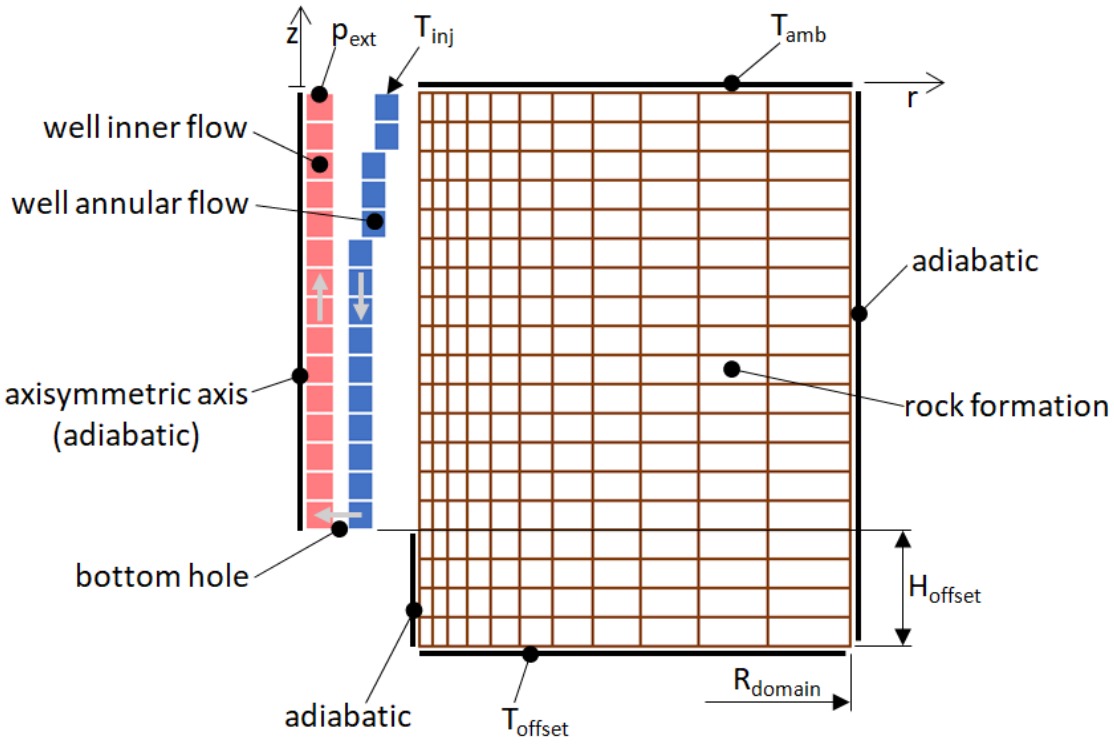

Figure 1. Boundary conditions and subdivisions of the domain: inner upstream, annular downstream and lithosphere.

As shown in Fig. 1, an extension of the lithosphere (H_{offset}) was deployed in the bottom boundary of the lithosphere domain, this aiming to avoid results deviations due numerical disturbances in the natural geothermal flow that comes upwards. The thermal properties of the well deepest rock type, found in the borehole logging, were considered for this extended portion. Then a Dirichlet condition was assumed for the domain bottom boundary surface (Fig. 1) and it was determined by an extrapolation of the Bottom Hole Temperature, as in Eq. (1):

$$T_{offset} = BHT^0 + \left|\nabla T_{geo}\right| \cdot H_{offset}. \tag{1}$$

Besides, the following assumptions were taken into account:

a) The thermal fluid cycling in the well is viscous liquid water, incompressible, with constant thermal conductivity and heat capacity;
b) Water constant properties (except viscosity) were taken from the average condition in temperature and pressure between the wellhead ($z = 0$) and bottom hole ($z = -H_{BH}$);
c) Annular and inner water flows are always fully developed, turbulent, one-dimensional with no edge effects;
d) The entire domain is axisymmetric, where the symmetry axis are coincident with the vertical axis of the well ($r = 0$, see Fig. 1);
e) So all the heat flows are considered in two directions, vertical ($\vec{z}$) and radial ($\vec{r}$);
f) Then the rock type in contact with the wellbore is horizontally considered the same along the lithosphere;
g) Only heat conduction is considered in the lithosphere domain (DiPippo, 2012, and Hamza *et al.*, 2005);
h) Only convective heat transfer is considered into the water flows and through their borders (pipe and casing walls) the heat flow is completely radial ($q_z^{"} = 0$);
i) All the finite elements were sized with constant height (Δz);
j) The finite elements of the water flow were vertically stacked and had the cross section varying as f(z), assuming the annular and inner areas for the corresponding depth of the well;
k) The lithosphere finite volumes were defined to have a proportion ratio between outer and inner radius ($f_r = r_o/r_i$);
l) Earth surface curvature and irregularities in the terrain were neglected;
m) The land surface temperature is assumed to be equal the ambient temperature (T_{amb}, see Fig. 1), a Dirichlet boundary condition;
n) The vertical boundary portions of the lithosphere that are not in contact with the wellbore are set to be adiabatic (Fig. 1);
o) Wellbore walls use L80 casings of diameters cataloged and defined in their borehole logging (SDT-ANP, 2017);
p) The production tubing is assumed as N80 pipe with diameter of 3 ½";
q) The surfaces of inner pipe and casing are uniform and with roughness of commercial steel tubes, $R_a = 0.046$ mm (White, 2011);
r) The production tubing (inner pipe) is externally coated with fiberglass, with thicknesses of ½", 1 ½" and 3" for depths corresponding to the well casing with diameters of 7", 9 $^5/_8$" and greater than 13" respectively;
s) The thermal capacities of pipes, thermal insulation and cementing are neglected, since the thermal inertia of the lithosphere is much greater than that of these components;
t) The thermal conductivities of fiberglass, cement and steel are considered constant and equal to 0.043, 0.72 and 42.2 W/m·K respectively (Bergman *et al.*, 2011).

The system of equations resulting from the domain discretization and conservative balances was solved using the Tridiagonal Matrix Algorithm, with root-mean-square of residual errors limited to 10^{-4}. It was coded in Fortran and it ran coupled to the Engineering Equation Solver (EES) software, from where the thermodynamic properties of the fluids were recovered.

Moreover, for each finite volume element of the water flow, the friction factor (f) was taken from the explicit formulation of Zigrang and Sylvester, Eq. (1), without considerable distortions in relation to the typical Colebrook's model (Genić, 2011):

$$f = \sqrt{-2 \cdot \log\left\{\frac{R_a}{3.7} - \frac{5.02}{Re} \cdot \log\left[R_a - \frac{5.02}{Re} \cdot \log\left(\frac{R_a}{3.7} + \frac{13}{Re}\right)\right]\right\}}, \qquad \text{where } \begin{cases} 4{,}000 \le Re \le 4 \cdot 10^8 \\ 0.00004 \le R_a \le 0.05\ (mm) \end{cases}. \tag{1}$$

An empiric formulation was also deployed to estimate the convective heat transfer, here calculated from the Gnelinsk expression for the Nusselt number (Bergman *et al.*, 2011), as

$$Nu = \frac{\frac{f}{8}(Re - 1{,}000) \cdot Pr}{1 + 12.7 \cdot \sqrt{\frac{f}{8}}\left(\sqrt[3]{Pr^2} - 1\right)}, \qquad \text{where } \begin{cases} 3{,}000 \le Re \le 5 \cdot 10^6 \\ 0.5 \le Pr \le 2{,}000 \end{cases}. \tag{2}$$

The initial temperature state (at $t = 0$), both for fluid and rocks, were set considering no thermal disturbance in the domain and proportional to the depth of each finite element ($T^0(z) = T_{amb} - |\nabla T_{geo}| \cdot z$). The pressure of the extracted water at the wellhead ($z = 0$) were set to a minimum value that assures no phase changing of the water while cycling inside the well. The water injection temperature depends on the ambient condition and performance of the power cycle coupled to the wellhead. These boundary conditions (p_{ext} and T_{inj}) are listed in the Tab. 3 and more detailed specifications about the power cycle are referred in the work of Batista (2019).

Table 3. Wellhead boundary conditions.

Case study	p_{ext} (kPa$_{abs}$)	T_{inj} (ºC)
MT	433.914	57.86
PR	408.475	55.88
RN	640.296	71.90
SC	555.229	66.59

Source: Batista (2019).

About the mesh (Δz, f_r) and domain (R_{domain}, H_{offset}) sizing, the coupled model were run for each location considering water overflow ($\dot{m}_{water} = 3$ kg/s), a long power plant lifecycle ($t = 30$ years) and reinjection temperature (T_{inj}) only 10ºC above the ambient condition. This to induce a higher thermal disturbance in domain than those actually could happen along the simulated geothermal power plant lifecycle, assuring mesh and domain sizing that could not deliver deviated results. Then sizing scenarios were plotted and evaluated to comply with the limits shown in Eq. (3):

$$\left|\frac{\partial}{\partial \lambda}\Phi(\lambda)\right| \leq 10^{-3}\,, \qquad \text{where } \Phi = T_{ext}, \dot{Q}_{well} \wedge \lambda = \Delta z, f_r, R_{domain}, H_{offset}\,. \tag{3}$$

Highlighting that extracted water temperature (T_{ext}) is one of the target outputs of the simulations, as well as the well heat power potential ($\dot{Q}_{well}$), which is defined as follows:

$$\dot{Q}_{well} = \dot{m}_{water} \cdot (h_{ext} - h_{inj}) \tag{4}$$

Furthermore, the temperature profile, $T(r, z)$, in the rock formation along the domain boundaries, away from the wall of the wellbore, also the geothermal heat flux (q''_{geo}) across the bottom surface of the model, must be equal the natural conditions of the earth crust in the respective well locations. Ultimately, the numeric models sizing were defined as listed in the Tab. 4.

Table 4. Mesh and domain size of the well numeric models.

Case study	Δz (m)	f_r	R_{domain} (m)	H_{offset} (m)	Volume elements counter
MT	24.91	1.271	94	229	6,325
PR	29.69	1.285	98	348	5,434
RN	39.74	1.254	76	342	3,282
SC	64.11	1.284	103	512	1,800

One last evaluation step was done, before running the year by year optimization on the water mass flow, it was about the error residual of the energy balance in steady state (when $t \to \infty$ and $a_{\Delta t} = 0$). Running the well AZ-II described by Noorollahi *et al.* (2015) in their work, the present numeric model delivered a residual of –0.23 kW, which corresponds to 0.8% of the entire heat rate supplied by the geothermal heat flow.

3. RESULTS

As presented in the Tab. 5, the simulated wells showed thermally affected zones (R_{TAZ}, where variation in temperature from the natural condition greater than 0.1% for any finite element) smaller than the domain size (R_{domain}). The natural temperature profile, $T_{geo}(z)$, is presented in Fig. 3, it corresponds to the state of the rocks distant from the wellbore (when $r \geq R_{TAZ}$) at any simulated time.

Besides, for any instant of time, the calculated geothermal heat flux was flat (and in the expected range as listed in the Tab. 5).

Table 5. Estimated thermal conditions for the Earth's crust.

Case study	R_{TAZ} (m)	calculated q''_{geo} (mW/m²)	reference q''_{geo} (mW/m²)(1)
MT	84.59	46.5	45 – 50
PR	86.39	60.7	59 – 63
RN	67.85	101.4	80 – 135
SC	92.23	113.8	80 – 135

(1)Source: IBGE (2010).

The water mass flow streaming in the wellbore was optimized, using embedded EES optimization algorithms, to maximize the net power output of the coupled power cycle (refer to Batista, 2019). This process delivered the water flow and corresponding extracted water temperature presented in Tab. 6.

Table 6. Optimized water flow and corresponding extracted water temperature.

	MT		PR		RN		SC	
t (year)	$\dot{m}_{water}$ (1)	T_{ext} (2)	$\dot{m}_{water}$ (1)	T_{ext} (2)	$\dot{m}_{water}$ (1)	T_{ext} (2)	$\dot{m}_{water}$ (1)	T_{ext} (2)
1/12	2.39	96.8	2.31	95.6	2.54	104.4	2.20	95.1
1	2.06	93.8	2.02	92.4	2.25	101.0	2.01	92.3
5	1.90	91.9	1.83	90.8	1.97	100.0	1.72	91.7
10	1.84	91.2	1.77	90.2	1.91	99.3	1.67	91.1
15	1.81	90.8	1.74	89.8	1.88	98.9	1.64	90.8
20	1.79	90.5	1.72	89.5	1.85	98.6	1.62	90.5
30	1.75	90.1	1.68	89.1	1.82	98.2	1.59	90.2

(1)(kg/s), (2)(ºC).

These conditions are consonant to the thermal energy profile, as shown in the Fig. 2, which also decreases over the simulated life cycle and trends to the steady state. It also infers the thermal behavior of the Earth's crust as a thermal capacitor, because the rate of geothermal heat supplied from the ground does not equate with the extracted heat power. This phenomenon is associated with the need to drill new wells in traditional geothermal plants from time to time (Gehringer, 2012).

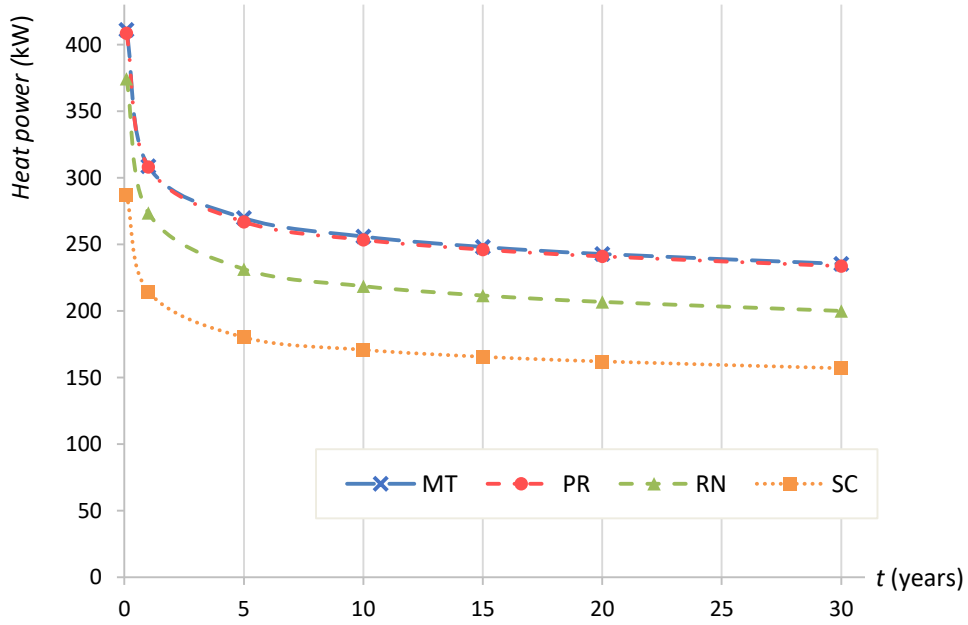

Figure 2. Heat power along the life cycle of the simulated geothermal wells.

The downstream water has a temperature drop as it flows through the top layers of the soil, as shown in Fig. 3. Only after depths around 3.1, 3.0, 2.8 and 2,7 km, for the wells MT, PR, RN and SC respectively, the downstream water reaches temperatures above T_{inj}. In other words, it is only from these depths that the system begins to have a positive balance of energy recovered from the lithosphere.

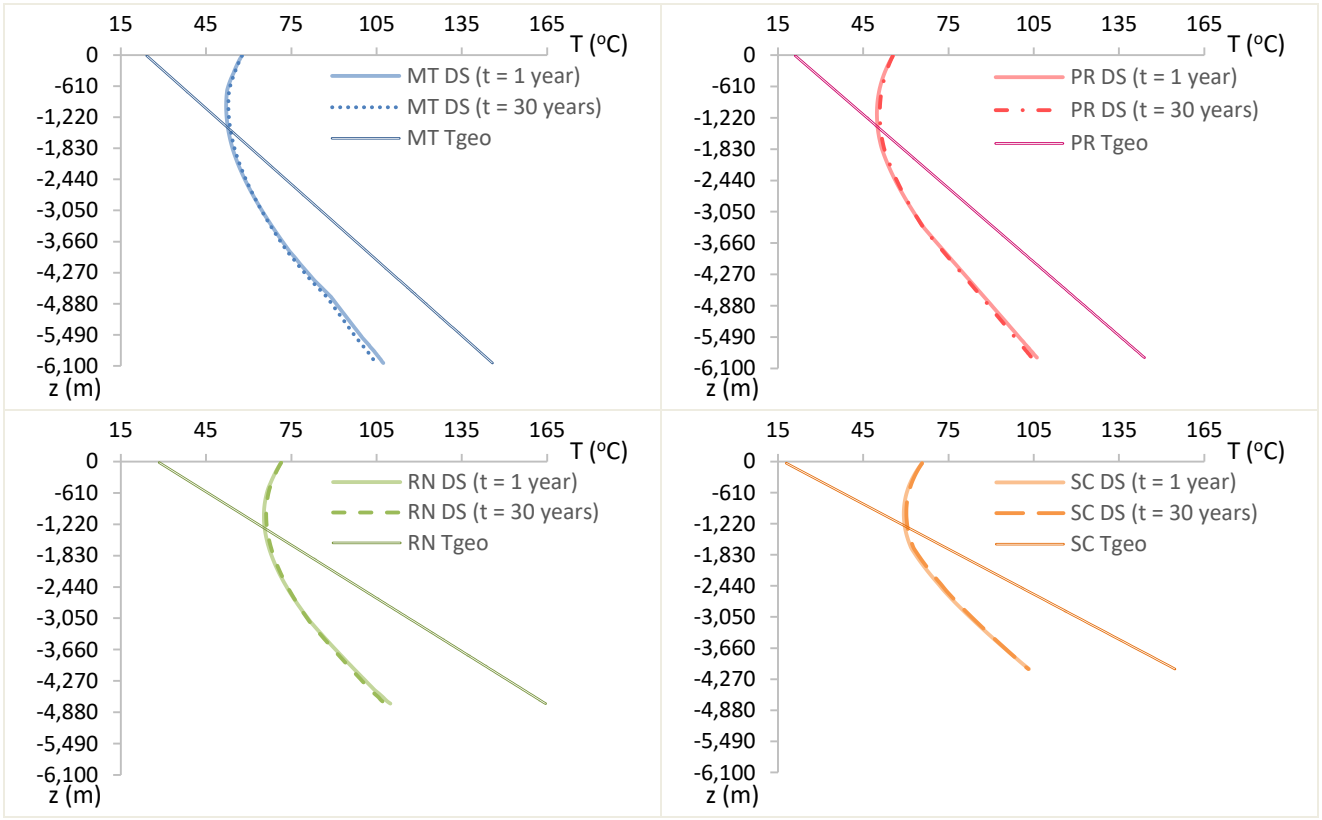

Figure 3. Natural temperature profile of the rocks and the water downstream temperature.

Moreover, as presented in Fig. 4, there is heat flow from the injected water to the higher portions of the soil, which is later dissipated to the atmosphere.

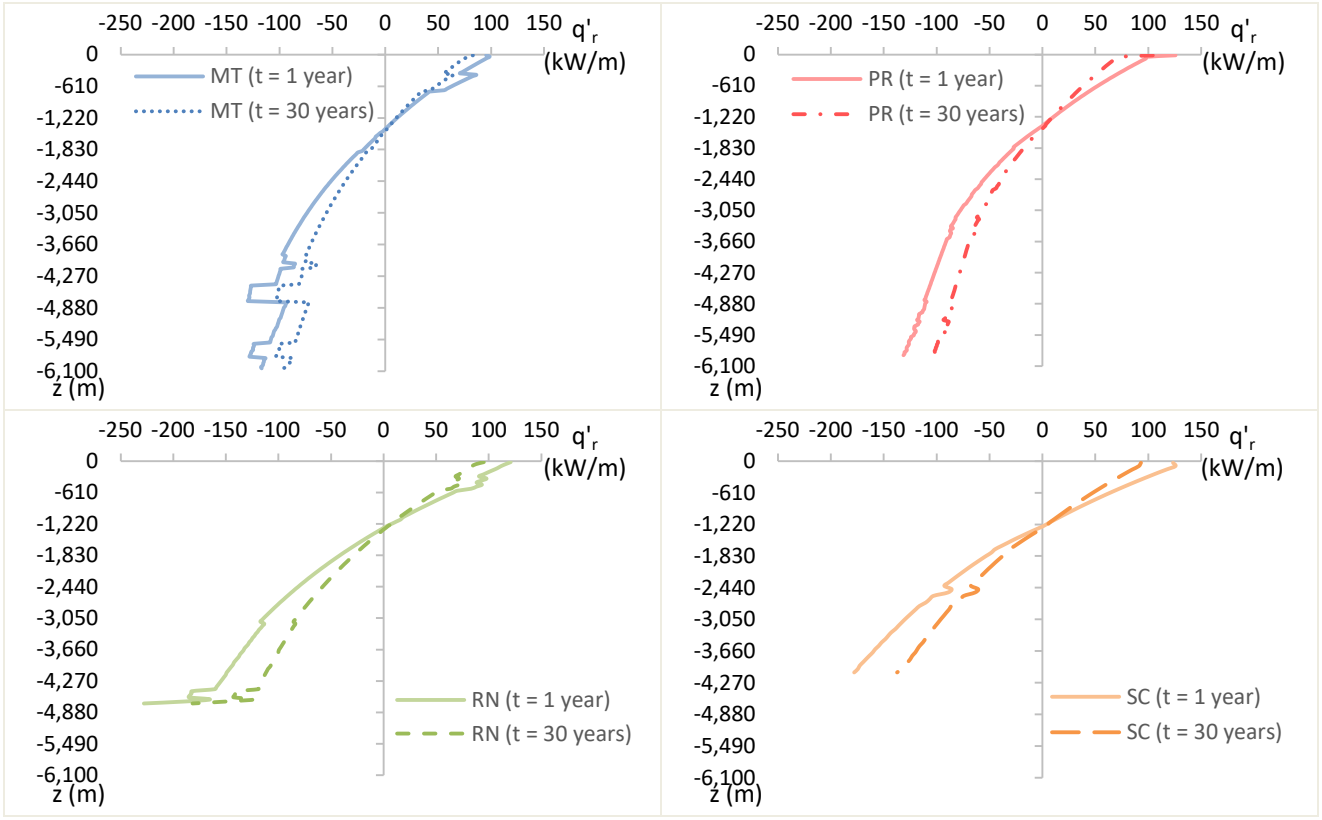

Figure 4. Heat rate trough the wall of the wells (positive for heat flowing from the annular flow to the rocks).

This heat loss to the surroundings occurs because it is not possible to take advantages of all exergy from the extracted water, since any proposed power cycle has limitations associated to its Pinch Point (refer to Batista, 2019), which defines T_{inj} greater than T_{amb}. For the studied cases, the losses reach values between 70 and 80 kW for the design point of the power cycle (set when $t = 1$ year).

Also, there is a heat flow from the water upstream, in the inner pipe, to the water downstream of the annular portion of the well. This heat rate is limited by the production tube insulation and, in total, varies between 1.33 and 4.68 kW along all the upstream, implying in decay in temperature of the water from the bottom hole to the wellhead (see Tab. 7).

.

Table 7. Bottom hole temperature and temperature loss along the water upstream.

	$t = 1$ year		$t = 30$ years	
Case study	BHT (ºC)	ΔT_{US} (ºC)	BHT (ºC)	ΔT_{US} (ºC)
MT	107.4	-13.6	104.8	-14.7
PR	106.1	-13.7	104.3	-15.2
RN	109.8	-8.8	108.2	-10.0
SC	103.3	-11.0	103.1	12.9

The water viscosity cannot be neglected, as it varies significantly along streams, as shown in Fig. 5, affecting the calculation of the Reynolds number (Re), and therefore the estimate for the friction factor (f) and the number of Nusselt (Nu). All the hydrodynamic and thermal problems are dependent on variations in viscosity.

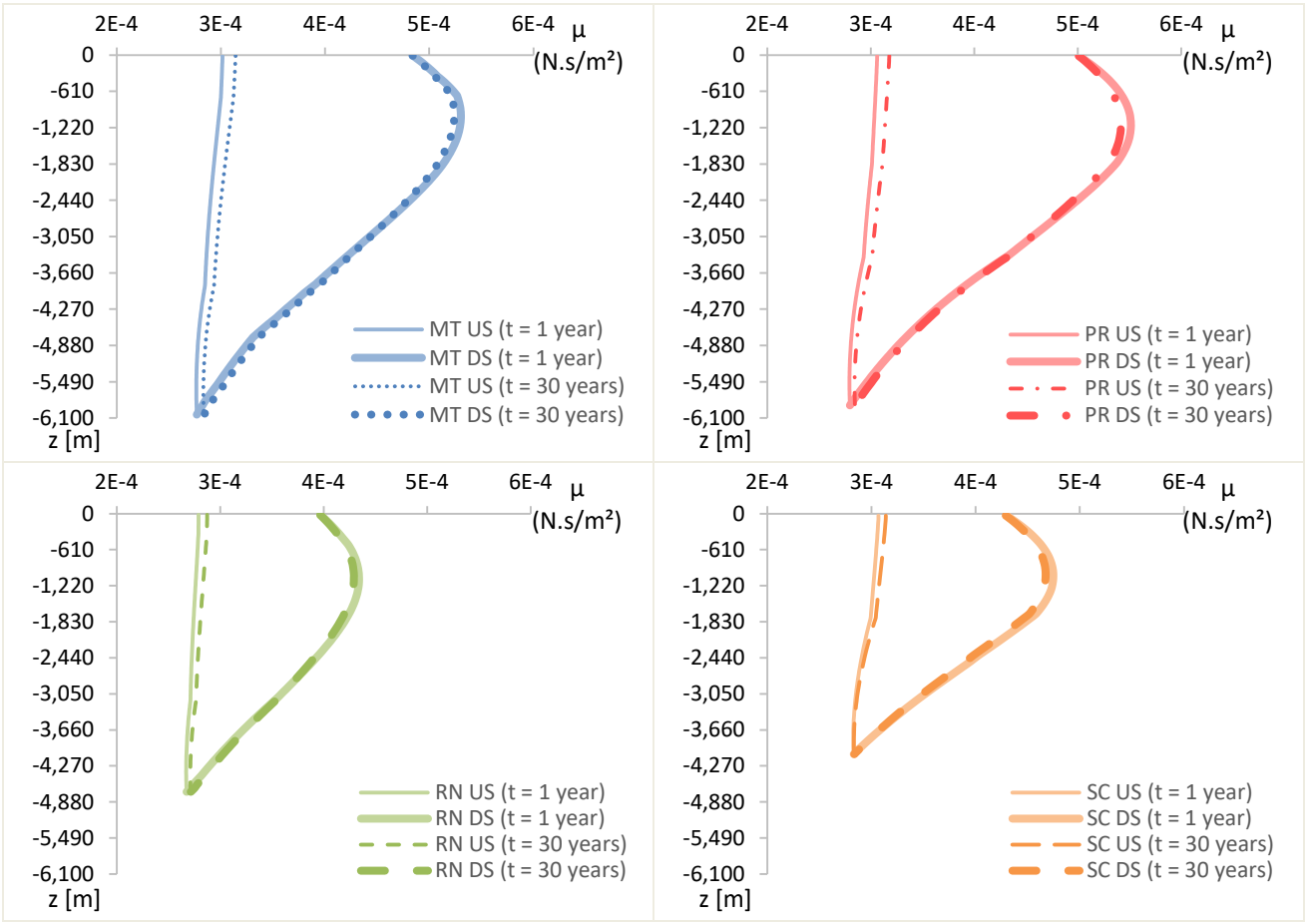

Figure 5. Water viscosity profile along the wells down and upstream.

The friction, along the water streams, converts the fluid potential energy into heat, resulting in pressure drop between the water inlet and outlet points, at the wellhead. This decay in pressure reaches values up to –1,008.09 kPa, as shown in Tab. 8, for the MT case. In this scenario, it may be required a water recirculation pump whose power is 2.35 kW (assuming pump efficiency of 90%). Moreover, the flow reaches high pressures in the bottom of the well. For the deepest case (MT) this pressure was estimated to be around 58.8 MPa_{abs}. Thus, these pressure load and loss conditions must be considered for the structure and equipment sizing of the wellbore.

Table 8. Pressure loss along the water stream and water pressure at the bottom of the well.

	$t = 1$ year		$t = 30$ years	
Case study	$\Delta p_{inj \to ext}$ (kPa)	p_{BH} (MPa_{abs})	$\Delta p_{inj \to ext}$ (kPa)	p_{BH} (MPa_{abs})
MT	-1,008.09	58.84	-759.09	58.80
PR	-1,041.53	57.43	-753.53	57.39
RN	-877.70	45.88	-602.70	45.84
SC	-945.28	39.95	-628.77	39.91

Lastly, when analyzing the fluid dimensionless numbers across the well domain and along all the simulated years, there are found values of Re and Pr ranging in 7,427 – 125,089 and 1.60 – 3.61 respectively, which ensure the applicability of empirical models described in Eq. (1) and Eq. (2). Also, Nu always varies between 44.94 and 398.90 for all simulated scenarios. This shows up that convective heat effects are much greater than the heat conduction into the water flows, confirming the possibility of simplifying the heat transfer model of the wellbore streams to be only convective, as it was done in the present work.

4. CONCLUSIONS

The present work aimed to evaluate the potential heat supply to four new geothermal power plants, hypothetically reusing abandoned oil wells located in the Brazilian states of Mato Grosso, Paraná, Rio Grande do Norte and Santa Catarina. The heat power of the wellbores was estimated between 287.4 and 411.0 kW after one month of operating time, decreasing to a range between 157.0 and 235.4 kW after 30 years.

It was verified over along the 30 simulated years, that the natural geothermal heat flow is not able to equate with the extracted heat power, which depletes the available heat stored in the rocks. This process tends to the steady state (which is not reached along the simulated life cycle) and shows up the behavior of the earth's crust as a thermal capacitor.

Also, it was found losses in the heat recovering process. The main heat loss is related to the temperature of the re-injected water, which implies in up to 80 kW of heat power dissipated to the soil. Regarding the production tube, there is a temperature decay about 8.8 – 15.2 ºC along it, from the heated water in the bottom hole to the wellhead. If considered the effects of pressure losses in the flow along the injection to the extraction point, that stream can be 12.5 km long for the deepest studied case, implying the need for a recirculation pump with power up to 2.35 kW.

Furthermore, it is recommended to validate the numerical model by simulating a real geothermal well deploying the double-pipe concept. Once it is not yet possible, some verification were carried out covering numerical convergence, mesh sizing influences, applicability of empirical formulations, size of the thermally affected zone, deviation on boundary elements conditions, residuals of energy balance in steady state and fluid properties variance. All of them indicated consistency of the applied modeling. Among these analyses, it is worth reinforcing the need to consider in this kind of problem the effects of friction inside the well, as well as variations in water viscosity along the flows.

5. ACKNOWLEDGEMENTS

The authors thank the National Superintendence of Technical Data (SDT) of the National Agency of Petroleum, Natural Gas and Biofuels (ANP) for supporting this research project in granting access to oil wells data. Also thanks to the Coordination for the Improvement of Higher Education Personnel (CAPES), for funding the scholarship to the Master student enrolled in this research project.

6. NOMENCLATURE

$\Delta p_{inj \to ext}$	Pressure drop from the water injection to extraction at the wellhead (kPa)
ΔT_{US}	Water upstream temperature difference, from the bottom hole to wellhead (ºC)
Δz	Height of each finite volume element (m)
λ	Generic mesh/domain sizing parameter
μ	Fluid absolute viscosity (N.s/m²)
ρ	Specific mass (kg/m³)
Φ	Generic target output
∇T_{geo}	Geothermal gradient (ºC/km)
$a_{\Delta t}$	Temporal component of the system of equations totally implicit, refer to Finite Volume Method
BHT	Bottom Hole Temperature (ºC)
BHT^0	Initial, or natural, Bottom Hole Temperature (ºC)
c_p	Specific thermal capacity (J/kg.K)
DS	Water downstream (annular flow)
f	Friction factor
f_r	Proportional ratio of the size of finite volume elements

h_{ext}	Specific enthalpy of extracted water at wellhead (kJ/kg)
h_{inj}	Specific enthalpy of re-injected water at wellhead (kJ/kg)
H_{BH}	Bottom hole depth (m)
H_{offset}	Height of the bottom domain extension (m)
k	Thermal conductivity (W/m.K)
$\dot{m}_{water}$	Mass flow rate of recirculating water (kg/s)
MT	Case study placed in the Brazilian state of Mato Grosso
Nu	Nusselt number
p_{BH}	Water pressure at the bottom hole (MPa_{abs})
p_{ext}	Pressure of extracted water (kPa_{abs})
Pr	Prandtl number
PR	Case study placed in the Brazilian state of Paraná
$q_r^{'}$	Radial, or horizontal, heat transfer rate per depth unit (W/m)
$q_{geo}^{"}$	Natural geothermal heat flux (W/m^2)
$q_z^{"}$	Vertical heat flux (W/m^2)
$\dot{Q}_{well}$	Heat power potential of the well (kW)
r	Radial, horizontal, distance from the axisymmetric axis (m)
r_i	Inner radius of each finite volume element in the lithosphere (m)
r_o	Outer radius of each finite volume element in the lithosphere (m)
$\vec{r}$	Perpendicular direction to the axisymmetric axis, horizontal
R_a	Arithmetical mean height (mm)
R_{domain}	Radius of the lithosphere domain (m)
R_{TAZ}	Radius of the thermally affected zone of the rocks domain (m)
Re	Reynolds number
RN	Case study placed in the Brazilian state of Rio Grande do Norte
SC	Case study placed in the Brazilian state of Santa Catarina
t	Elapsed operation time (years)
T^0	Initial temperature condition (ºC)
T_{amb}	Atmospheric temperature (ºC)
T_{DS}	Temperature of the water downstream (ºC)
T_{ext}	Temperature of extracted water (ºC)
T_{geo}	Natural temperature profile of the lithosphere (ºC)
T_{inj}	Temperature of re-injected water (ºC)
T_{offset}	Temperature of the bottom boundary surface of the domain (ºC)
US	Water upstream (inner flow in the production tube)
z	Vertical distance from the axisymmetric axis (m)
$\vec{z}$	Direction of the axisymmetric axis, vertical

7. REFERENCES

Barcelos, J.G.A.., 2017. *Modelagem matemática do aumento de pressão nos anulares (APB) em poços de petróleo*. Master's dissertation, Universidade Federal de Santa Catarina, Florianópolis, Brazil.

Batista, T.C., 2019. *Pré-viabilidade de usinas geotérmicas em poços de petróleo terrestres abandonados no Brasil*. Master's dissertation, Universidade Federal de Santa Catarina, Florianópolis, Brazil.

Bergman, T.L., Incropera, F.P., DeWitt, D.P., Lavine, A.S., 2011. *Fundamentals of Heat and Mass Transfer*. John Wiley & Sons, 7th edition.

Bu, X., Ma, W., Li, H., 2012. "Geothermal energy production utilizing abandoned oil and gas wells". *Renewable Energy*, Vol. 41, pp. 80–85, 2012

Cheng, W.L., Li, T.T., Nian, T.L., Wang, C.L., 2013. "Studies on geothermal power generation using abandoned oil wells". *Energy*, Vol. 59, pp. 248–254.

Davis, A.P., Michaelides, E.E., 2009. "Geothermal power production from abandoned oil wells". *Energy*, Vol. 34, No. 7, pp. 866–872.

Dipippo, R., 2012. *Geothermal Power Plants: Principles, Applications, Case Studies and Environmental Impact*. Butterworth-Heinemann, Waltham, 3rd edition.

ESMAP, 2012. *Geothermal Handbook: Planning and Financing Power Generation*. The International Bank for Reconstruction, Washington, Technical Report No. 002.

Genić, S., Arandjelović, I., Kolendić, P., Jarić, M., Budimir, N., Genić, V., 2011. "A Review of Explicit Approximations of Colebrook's Equation". *FME Transactions*, Vol. 39, pp. 67–71.

IBGE, 2010. *Atlas nacional do Brasil Milton Santos*. IBGE - Diretoria de Geociências, Rio de Janeiro.

Hamza, V.M., Dias, F.J.S., Gomes, A.J.L., Terceros, Z.G.D., 2005. "Numerical and functional representations of regional heat flow in South America". *Physics of the Earth and Planetary Interiors*, Vol. 152, pp. 223-256.

Maliska, C.R., 2004. *Transferência de calor e mecânica dos fluidos computacional*. LTC, Rio de Janeiro, 2nd edition.

Merkel, A., 2017. "Climate-Data.org". AM Online Projects. 07 Jul. 2017 <https://climate-data.org>.

Noorollahi, Y., Pourarshad, M., Jalilinasrabady, S., Yousefi, H., 2015. "Numerical simulation of power production from abandoned oil wells in Ahwaz oil field in southern Iran". *Geothermics*, Vol. 55, pp. 16–23.

REN21, 2017. *Renewables 2017 Global Status Report*. REN21 Secretariat, Paris. Technical Report.

Schön, J., 2015. *Physical Properties of Rocks: Fundamentals and Principles of Petrophysics*. Elsevier, 2nd edition.

SDT-ANP. "Banco de Dados de Exploração e Produção (BDEP)". Agência Nacional de Petróleo, Gás Natural e Biocombustíveis. 07 Jul. 2017<http://www.anp.gov.br/exploracao-e-producao-de-oleo-e-gas/dados-tecnicos/acervo-de-dados>.

White, F.M, 2011. *Fluid mechanics*. McGraw-Hil, New York, 7th edition.

Wight, N.M., Bennet, N.S., 2015. "Geothermal energy from abandoned oil and gas wells using water in combination with a closed wellbore". *Applied Thermal Engineerin*g, Vol. 89, pp. 908–915.

Yang, Y. Huo, Y., Xia, W., Wang, X., Zhao, P., Dai, Y., 2017. "Construction and preliminary test of a geothermal ORC system using geothermal resource from abandoned oil wells in the Huabei oilfield of China". *Energy*, Vol. 140, pp. 633–645.

8. RESPONSIBILITY NOTICE

The authors are the only responsible for the printed material included in this paper.